Dinku *et al. Appl Biol Chem* (2020) 63:16
https://doi.org/10.1186/s13765-020-00499-w

KSABC
The Korean Society for Applied Biological Chemistry

ARTICLE Open Access

Anti-proliferative activity of a novel tricyclic triterpenoid acid from *Commiphora africana* resin against four human cancer cell lines

Worku Dinku[1], Johan Isaksson[2], Fredrik Garnås Rylandsholm[2], Petr Bouř[3], Eva Brichtová[3,4], Sang Un Choi[5], Sang-Ho Lee[5], Young-Sik Jung[5], Zae Sung No[6], John Sigurd Mjøen Svendsen[2], Arne Jørgen Aasen[2] and Aman Dekebo[1*]

Abstract

Myrrh, a resin derived from the damaged bark of *Commiphora* genus, has traditionally been used for treatment of various human diseases, such as amenorrhea, ache, tumors, fever, and stomach pains. In spite of this widespread use of the myrrh in Ethiopia, the pharmacological activity and chemical composition have not been studied in detail. A new tricyclic triterpene acid (3*S*,4*S*,14*S*,7*E*,17*E*,21*Z*)-3,30-dihydroxypodioda-7,17,21-trien-4-carboxylic acid (commafric A) has been isolated from a crude methanolic extract of *Commiphora africana* (A. Rich.) Engl. resin along with the known pentacyclic triterpene α-amyrin. The structure of commafric A was characterized using different spectroscopic techniques such as 1D and 2D NMR, IR, and VCD combined with computations. The anti-proliferative activity of both isolated compounds was evaluated using SRB based colorimetric cellular assay against four human cancer cell lines. Etoposide was used as a positive control. Commafric A showed significant anti-proliferative effects against non-small cell lung cancer (A549) with IC_{50} values of 4.52 µg/ml. The pentacyclic triterpene α-amyrin showed a weak anti-proliferative activity against A2780 (ovarian cancer), MIA-PaCa-2 (pancreatic cancer), and SNU638 (stomach cancer) cell lines tested with IC_{50} values ranging 9.28 to 28.22 µg/ml. Commafric A possessed anti-proliferative activity against non-small cell lung cancer (A549), which suggests that commafric A has potential to be further optimized being a lead compound in the search for new drugs against cancer diseases.

Keywords: *Commiphora africana*, Commafric A, Anti-proliferative, SRB, A549 cell line

Introduction

Natural products are very inspiring in the drug discovery process. Aziz et al. [1] reviewed several drugs that have been obtained from different plant sources. Some of them can be obtained from *Commiphora africana* (A. Rich.) Engl. (Burseraceae), which is a bush about 1.5 m tall and is wide-spread in African countries, such as Sudan, Ethiopia, Eritrea, Somalia, Kenya, Uganda, and Mozambique [2]. Roots, bark and leaves are traditionally used to treat measles, hyperlipidemia, and cardiovascular disorders [3, 4]. The leaves are also used as a sedative and soporific [3], and the resin is used for antiseptic washes and baths to treat skin infections, sores, and leprosy [5]. Ethnobotanical information has indicated that bark, resin, and leaves of *C. africana* are used to treat snakebite, skin wounds, tumor, stomachache, and as anti-ticks [6]. A fraction obtained after partitioning the crude ethanolic extract roots of *C. africana* exhibited a promising in vitro antimicrobial activity [4].

The resin of *C. africana* contains betulin [7], which has been shown to have antitumor activity, especially in combination with cholesterol [8]. Betulinic acid derivatives can inhibit HIV-1 [9]. Other *Commiphora* species

*Correspondence: amandekeb@gmail.com
[1] Department of Applied Chemistry, Adama Science and Technology University, Adama, Ethiopia
Full list of author information is available at the end of the article

have also provided pharmaceutically interesting compounds. Furanoeudesma-1,3-diene, the major compound of myrrh [10, 11], has been reported to exhibit analgesic activity in mice [12].

Previously, we have described oxygenated furanosesquiterpenes, curzerenone, and furanodienone from the resins of *C. sphaerocarpa* (Chiov.), *C. holtziana* (Engl.), and *C. kataf* [11, 13, 14]. Messina et al. [15] has shown that furanodienone has anti-inflammatory, antimicrobial, and anticancer activities. Additionally, the cytotoxicity of nordammarane triterpenes, such as vibusambucin A, 12β-hydroxy-3,15-dioxo-20,21,22-23,24,25,26,27-octanordammarane, and hupehenol A against KB, HepG-2, LU-1, and MCF-7 cell lines has been reported [16]. The resins of *C. confusa* contain triterpenes of the dammarane type [17] with moderate cytotoxic activity against HepG2 [18]. From the resin of *C. erlangeriana* we have previously isolated polygamain-type lignans named erlangerin A, and erlangerin B, and two lignans related to podophyllotoxin, erlangerin C, and erlangerin D [19]. The effects of the erlangerins C and D are closely related to those of podophyllotoxin. They induce concentration-dependent cytotoxicity in the murine macrophage cells (RAW 264.7) and a cytostatic effect in HeLa, EAhy926, and L929 cell lines [20].

In spite of the use of *Commiphora africana* in traditional medicine, to the best of our knowledge, there has been no study aimed at isolation and characterization of anti-proliferative constituents of this plant. As part of the exploration of the pharmacological potential of the resins from *Commiphora* genus, we herein report the isolation, structural elucidation, and anti-proliferative activity screening of a new oxygenated podioda-7,17,21-triene [21, 22] and α-amyrin obtained from *C. africana.*

Materials and methods

Plant material

Resins and botanical specimens of *C. africana* were collected from district of Yabello, Borena zone, Ethiopia in December 2016 and identified by a botanist Shambel Alemu at the Biology Department, Addis Ababa University. A voucher specimen has been deposited at the National Herbarium (number: 072801) of Addis Ababa University, Addis Ababa, Ethiopia. This tree is known by its vernacular name HAMMESA DIHRO (Afaan Oromo). There is no permission required to collect samples from wild to investigate their chemical composition and evaluate their anti-proliferative effects.

Extraction and isolation

The resin (322.5 g) of *C. africana* was air dried and extracted with methanol (1 L × 3) for 3 days at 25 °C. The solvent was removed *in vacuo* to yield a yellow extract (151.2 g, 46.82%). The extract (80.0 g) was suspended in water (800 ml) and successively partitioned with *n*-hexane (800 ml × 3), chloroform (800 ml × 3), EtOAc (800 ml × 3), and *n*-BuOH (800 ml × 3) yielding an *n*-hexane (33.39 g, 40.22%), a chloroform (41.26 g, 49.7%), an EtOAc (0.11 g, 0.132%), and an *n*-butanol fraction (0.074 g, 0.093%). Part of the *n*-hexane fraction (7 g) was flash chromatographed on a silica gel column using *n*-hexane/EtOAc (7:3) as an eluent furnishing commafric A (**1**) (430 mg), and α-amyrin (**2**) (22 mg) (Fig. 1).

General experimental procedure

Melting points are uncorrected. TLC was performed on precoated plates (Silica gel 60 F_{254}, Merck) using *n*-hexane/EtOAc/MeOH (10:10:0.1) as a developing solvent and with vanillin-H_2SO_4 as the detecting reagent. CC was performed on silica gel. IR spectra were measured on a Perkin Elmer 1600 instrument using KBr tablets. Optical rotation was measured on a Perkin-Elmer 241 polarimeter. UV spectra were recorded on a Shimadzu UV–VIS spectrophotometer. LC-Mass was acquired on Waters ACQUITY H-CLASS Liquid Chromatograph/SQD2 Mass Spectrometer; Injection mode: FIA, Eluent: Methanol/Water (10 mM ammonium acetate) = 70/30 flow rate: 0.3 ml/min, Ionization mode: ESI (positive), Capillary voltage: 3 kV, Cone voltage: 30 V. HRESIMS data were obtained on Waters ACQUITY UPLC I - Class Liquid Chromatograph/TQ-S micro Tandem Mass-Spectrometer, Ionization mode: electrospray ionization (ESI), Mass Analyzer, JMS-700 Mass High Resolution Mass Spectrometer (Jeol LTD, Tokyo, Japan): Tandem (triple) quadrupole at mass range of 5–2000 m/z and scan speed 15,000 Da/sec.

Nuclear magnetic resonance spectroscopy

^1H and ^{13}C NMR data for commafric A (**1**) was acquired on an Avance III HD spectrometer (Bruker-BioSpin GmbH, Germany) equipped with an inverse detected TCI cryoprobe with a cryogenic enhancement for ^1H, ^2H, and ^{13}C, operating at 600 MHz for ^1H. All spectra were recorded using TopSpin 3.5pl7 at 298 K in dichloromethane-d_2 and chloroform-d_1, using gradient selected and adiabatic inversion versions of pulse sequences where applicable. Analysis of *NOE* buildup for compound **1** was performed by complete relaxation matrix analysis using Mspin 2.3.2-694 (MestreLab Research S. L., Spain). The results are presented as Boltzmann averaged *NOE* enhancement across the conformational ensemble generated for analysis of IR and VCD section. The sample for anisotropic NMR measurements (10 mg) was dissolved in $CDCl_3$ with 0.03% TMS to which increasing amounts

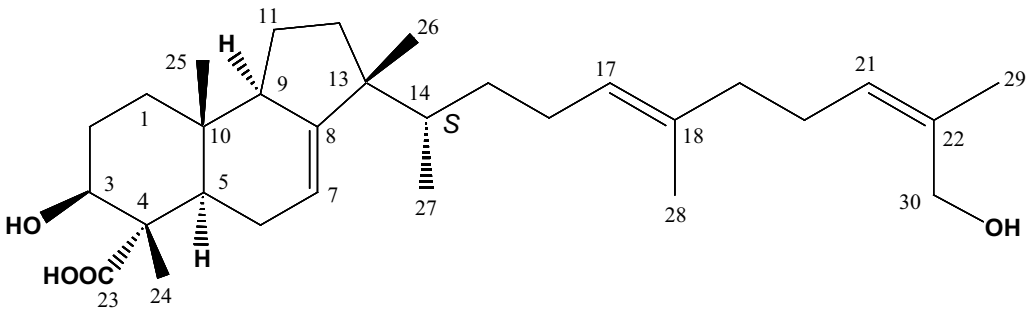

Commafric A (**1**)

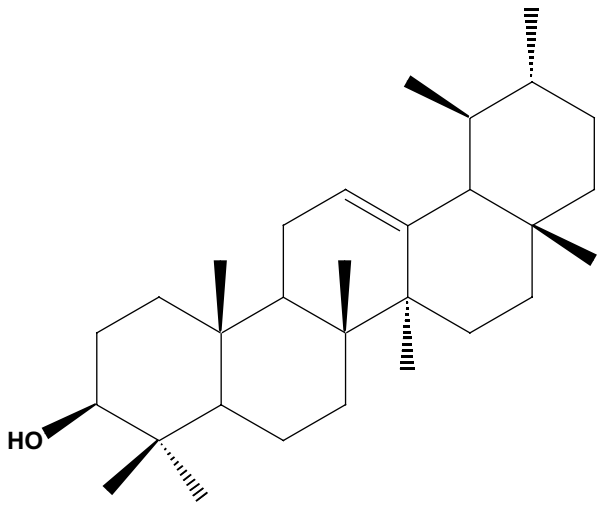

α-amyrin (**2**)

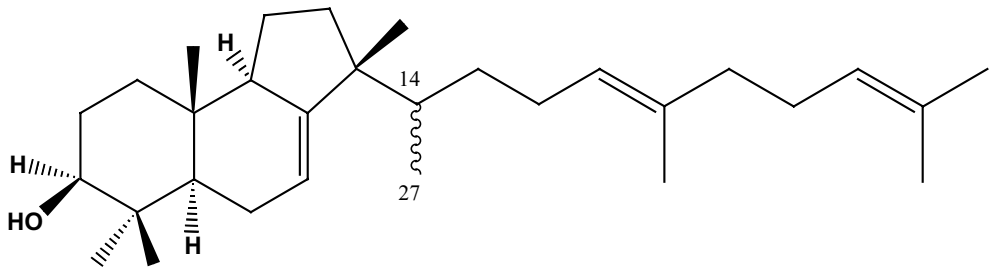

Podioda-7,17,21-trienol (**3**)

Fig. 1 Chemical structures of compounds isolated from *C. africana* and a reference compound podioda -7,17,21-trienol (**3**)

of poly-γ-benzyl-L-glutamate (PBLG, 150,000–300,000 Da, Sigma-Aldrich CAS 25014-27-1) was added to yield weight-to-volume ratios of 7.9%, 12.1%, and 16.2%. For compound **1** 1D carbon, CLIP-HSQC, IPAP-HSQC, and J-res carbon was acquired to extract the $^{1}J_{CH}$ coupling constants and anisotropic carbon shifts. The data treatment is thoroughly described in additional file.

Experimental vibrational circular dichroism (VCD) spectra

VCD and absorption spectra of **1** were measured in $CDCl_3$ solutions (~1 mg/100 µl) using a BaF_2 cell of an optical path of 50 µm and a BioTools ChiralIR-2X

instrument. Spectra of pure $CDCl_3$ solvent were subtracted as a baseline; the accumulation time was ~ 12 h using blocks of 1200 scans and 4 cm^{-1} resolution.

Computations

Using the Gaussian suite of programs [23] a systematic conformer search of compound **1** was performed considering the three torsional angles in the vicinity of the tricyclic system. Other C–C–C–C dihedral angles were all-*trans* and all-extended (180°) at the beginning of the optimizations and left to optimize without constraints. The B3LYP [24] PCM [25] (chloroform)/6–31++G** level was used for all quantum chemistry. For stable conformers thus obtained the magnetic field perturbation theory [26, 27] was used to simulate IR and VCD intensities; final spectra were obtained as a Boltzmann average, using a convolution with Lorentzian lines (FWHM = 10 cm^{-1}). Since the consideration of the full molecular flexibility was not possible with our computational means, atomic axial tensors of the linear side chain (from carbon number 16) were deleted for VCD generation. The chain itself is not chiral and thus supposedly the error introduced by this approximation is small, whereas the dominant signal from the chiral more rigid molecular part may help to assign the absolute configuration. Alternated simulations of the spectra based on molecular dynamics were attempted as well, but did not provide results significantly different from the limited conformer model. Boltzmann-averaged isotropic shielding and spin–spin coupling constants were computed at the same level as for VCD.

Tumor cell lines

The cell lines used in this study were the human non-small cell lung cancer cell lines (A549), ovarian cancer cell line (A2780), pancreatic cancer cell line (MIA-Paca-2), and stomach cancer cell line (SNU-638), and they were maintained using RPMI1640 cell growth medium (Gibco, Carlsbad, CA), supplemented with 5% fetal bovine serum (FBS) (Gibco), and grown at 37 °C in a humidified atmosphere containing 5% CO_2 [28]. All the cancer cells used were adapted for 6 months at least to the RPMI1640 medium at Korea Research Institute of Chemical Technology, then used in the anti-proliferative assays. Cells were exposed to the isolated compounds at concentrations ranging from 0.1 to 30 µg/ml.

Anti-proliferative assessment

All experiments were conducted by the NCI's protocol [28]. Experimental cultures were placed in 96-well microtiter plates (Corning) containing 0.15 ml of growth medium per well with a cell density of 5×10^3 (A549, A2780, and MIA-Paca-2) and 1×10^4 (SNU-638). The culture was incubated at 37 °C and humidified by 5% CO_2 for 1 day. Then, media were aspirated off and added the test material in triplicate which was dissolved in media at varying concentrations. In case of necessity, the test material was dissolved in small amount of dimethyl sufoxide (DMSO), but the final concentration of DMSO in the medium did not exceed 0.5%. The culture was incubated for additional 3 days. After 3 days of continuous drug exposure, the medium was removed by flicking plates over a sink. The cells attached to the plastic substratum were fixed by gently layering with 0.1 ml of cold 10% trichloroacetic acid (TCA). Incubation at 4 °C for 1 h was followed by wash with tap water five times to remove TCA solution. After being washed and dried at RT overnight, TCA fixed cells were stained with 0.1 ml of 0.4% sulforhodamine B (SRB) in 1% acetic acid per well for 30 min. At the end of the staining period, SRB supernatant was removed and the remaining cells were rinsed with 1% acetic acid five times. It was dried until no standing moisture was visible, and then the bound dye in cells was extracted with 0.1 ml of l0 mM unbuffered Tris base (pH 10.5) per well by stirring on a gyratory shaker for 5-10 min, followed by measured the optical density at 520 nm by MR700 microplate reader (Dynatech Laboratories). Antitumor activity of the test material at varying concentrations was estimated as the net growth % of cells compared with that of control (without test material, net growth = 100%). The dose–response curves of test material were constructed and the IC_{50} value was calculated as the concentration of the test material that caused 50% inhibition of cell growth against the cancer lines A549, A2780, MIA-PaCa-2, and SNU638. Etoposide, a standard drug was used as a positive control. IC_{50} values of etoposide were compared with those for crude extract, *n*-hexane fraction, and isolated compounds.

Results

Isolation of compounds

Flash column chromatography of the *n*-hexane fraction using *n*-hexane/EtOAc (7:3) as an eluent furnished two pure compounds: commafric A (**1**) the most abundant isolated molecule and the known compound α-amyrin (**2**), were obtained as white solids. The structures of the isolated compounds were elucidated employing ^{13}C and ^{1}H-NMR as well as 2D-NMR, IR, FT-ESI–MS mass fragmentation pattern, and comparing with literature data reported for structurally related compounds. The ^{1}H NMR and ^{13}C NMR data of compound **2** agreed with corresponding published data for α-amyrin (**2**) [29–31].

Characterization of compound 1

Compound **1** was obtained as a white powder (mp 126–127 °C), with $[\alpha]_D^{22}$: +4° (*c* 1.0, $CHCl_3$) and its

molecular formula was established on the basis of a high resolution positive-ion mode HR-ESI-MS^2 scanned from 170.00 to 600.00 m/z. The molecular formula was established as $C_{30}H_{48}O_4$ on the basis of the positive-ion mode HRESIMS data due to Na adduct formation (m/z 495.3442 $[M+Na]^+$, calcd. 495.3445) and NMR data indicating seven degrees of unsaturation (Additional file 1: Fig. S1). The two peaks with less intensity at *m/z* 473.36 and *m/z* 455.3515 corresponds to protonation of the molecule $[M+H]^+$and protonation of a dehydrate molecule respectively (Additional file 1: Fig. S1).

The UV spectrum of **1** (EtOH) exhibited an absorption band at 209 nm indicating the absence of conjugated double bonds. The experimental IR-spectrum agrees with the simulated spectrum of commafric A (Fig. 2); the most prominent features comprise free (3607 cm^{-1}) and hydrogen-bonded (3400 cm^{-1}) OH stretching bands, split (2956/2872 cm^{-1}) CH stretching signal indicating the presence of both sp^2 and sp^3 carbons, and the C=O stretching band (1695 cm^{-1}).

^{1}H NMR resonances (Table 1) of **1** included two near triplets at δ_H 5.30 and 5.04, and one doublet of a triplet at δ_H 5.16, suggesting the presence of three olefinic protons. Two geminally coupled protons appearing as doublets at δ_H 4.17 and 4.07 indicated the presence one oxy methylene moiety. A signal integrated as one proton at δ_H 4.02 suggested the presence of an oxy methine group. Two moderately deshielded methyl signals were observed (1.57 and 1.77 ppm), indicating that two methyls are attached to sp^2 hybridized carbons (see Additional file 1: Fig. S2). Additionally, the compound has four aliphatic methyl signals (0.75, 0.86, 0.91, and 1.18).

The ^{13}C NMR (Table 1 and Additional file 1: Fig. S3) and multiplicity edited HSQC/DEPT confirmed the presence of thirty carbons, of which seven were quaternary, ten methylene, seven methine, and six methyl groups. A set of 2D NMR experiments, HSQC, HMBC, H2BC, HSQC-TOCSY, DQF-COSY, and 1,1-ADEQUATE (Additional file 1: Fig. S4–S9), was used to establish the molecular framework of commafric A as a tricyclic triterpenoid with structural similarity to podioda-7,17,21-trienol [21]. All carbon–carbon connections were unambiguously confirmed by 1,1-ADEQUEATE, except for the two quaternary to quaternary carbon bonds (C4 to C23 and C8 to C13), which did not correlate in this pulse sequence because of the absence of protons on both sides of the C–C bond (Fig. 3b). The C23 carboxyl group could be placed by HMBC correlations to H3, H5, and H24 from C23, while the C8 to C13 bond was confirmed by HMBC correlations between H26 and H12, and C8. The location of the hydroxymethylene group as well as the position of the 21, 22 double bond was confirmed by 2D HMBC (Fig. 3a), which showed three bond couplings between the olefinic proton H21 (δ_H 5.30) and the carbons at the C29 methyl group (δ21.4) and the C30 hydroxymethylene carbon (δ_C 61.5). Furthermore, H2BC two-bond couplings appeared between C22 and Me29 and hydroxymethylene protons H30′/″ (Fig. 3a).

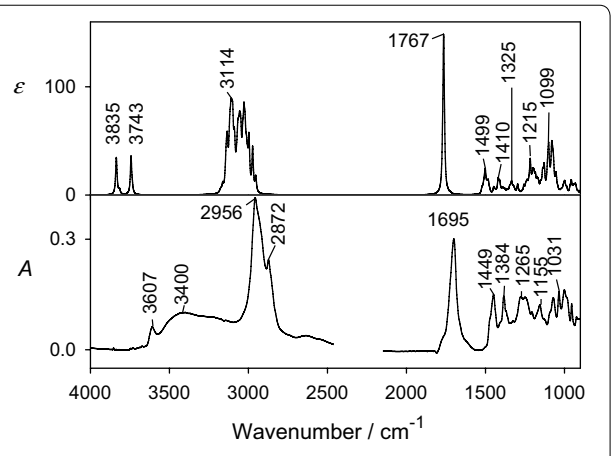

Fig. 2 Calculated (upper panel, raw DFT frequencies) and experimental (lower panel) IR spectra of commafric A

Determination of the relative configuration

Based on $^3J_{CH}$ couplings measured by selective CLIP-HSQMBC [32], as well as NOESY/ROESY analysis, the C17/C18 configuration was determined as *E* ($^3J_{C28H17}$ = 8.0 Hz and $^3J_{C19H17}$ = 6.0 Hz) and the C21/C22 configuration was determined as *Z* ($^3J_{C29H21}$ = 6.0 Hz and $^3J_{C30H21}$ = 9.3 Hz, Additional file 1: Figs. S10–S12). These conclusions are based on the fact that the *trans*-$^3J_{CH}$ is expected to be stronger than the corresponding *cis*-$^3J_{CH}$. This was also consistent with the direct observations of the presence of the NOE_{H21H29} and ROE_{H21H29}correlations, and the absence of the NOE_{H21H29} and ROE_{H21H29} correlations. The *Z*-configuration of the C21 to C22-double bond is also consistent with the ^{13}C NMR chemical shifts of C21, C22, C29, and C30 in previously reported compounds with similar side chain configurations [33, 34].

The relative configuration of the tricyclic system was established by NOESY and ROESY correlations (Additional file 1: Fig. S12) supplemented with some $^3J_{HH}$ and $^3J_{CH}$ couplings. Most notably, an N/ROE correlation trace between H3–H5–H9–H11″–H12″ place these protons below the ring plane while the trace between H24–H25–H11′–H12′–H26 place these above the ring plane. The key correlations are displayed in Fig. 3c. The configuration at the C14 stereocenter could not be unambiguously determined from the N/ROE correlations without a full conformational analysis because of relatively free rotation about the C13–C14 bond.

Table 1 NMR parameters of commafric A in CD_2Cl_2:^1H (600 MHz) and ^{13}C (150 MHz) NMR, HMBC, H2BC, ADEQUATE-1,1, and ROESY

No.	δ_C	δ_H (multi, J in Hz)	HMBC (H → C)[d]	H2BC (H → [H]C)[d]	1,1-ADEQUATE ([H]C → C)[d]	Key ROESY
1	38.1	1.72 (dt, *J* = 13.3, 3.1)/1.32 (m[c])	25	2‴	2‴	2′‴, 25, 2′/‴
2	27.3	1.67 (m[c])	3	1′, 1″, 3	1′, 1″, 3	1′‴, 25
3	76.2	4.02 (dd, *J* = 11.2, 4.7)	1″, 2″, 5, 24	2‴	2‴	2′‴, 5
4	52.9		2′, 2″, 3, 5, 24		3, 5, 24	
5	46.6	1.88 (m[c])	24, 25	6′, 6″	6′, 6″	3, 9
6	25.8	2.05 (m[c])/1.80 (m[c])		5, 7	5, 7	7, 24, 25
7	114.0	5.16 (dt, *J* = 5.1, 2.6)	6′	6′, 6″	6′, 6″	14
8	151.0		6′‴, 11′‴, 12′‴, 26		7, 9	
9	59.5	2.01 (m[c])	1′, 5, 11′ ,12′‴ ,25	11′, 11″	11′, 11″	1″, 5, 11″, 12″
10	34.1		1′‴, 5, 25		1′, 1″, 5, 9, 25	
11	23.1	1.25 (m[c])/1.53 (m[c])	12′‴	12″	9, 12′, 12″	25, 26/9
12	33.0	1.25 (m[c])/1.48 (m[c])	11′‴, 14, 26[a]	11′, 11″	11′, 11″	26/9, 15′/‴, 27
13	48.3		12″, 14, 26, 27		12′, 12″, 14, 26	
14	41.2	1.36 (m[c])	9, 12″, 26, 27	15′, 27	15′, 27	6′, 6″, 7
15	33.0	1.34 (m[c])/1.00 (m[c])	16″, 27[a]	14, 16′, 16″	14, 16′, 16″	
16	26.6	2.02 (m[c])/1.87 (m[c])	15′‴, 17[b]	15″, 17	15′, 15″, 17	
17	125	5.04 (ddq, *J* = 7.5, 6.3, 1.3)	15′‴, 16′‴, 19′‴, 28	16′, 16″, 28*	16′, 16″	
18	135		16′‴, 19′‴, 28		17, 19′, 19″, 28	
19	40.0	1.96 (m[c])/1.93 (m[c])	20″, 28, 29	20′, 20″	20′, 20″	
20	26.7	2.14 (m[c])/2.09 (m[c])	21[b]	19′, 19″, 29**	19′, 19″, 21	
21	129.0	5.30 (t, *J* = 7.0)	19′‴, 20′‴, 29, 30′‴	19′, 19″, 29*	20′, 20″	29
22	134.0		20′‴, 29, 30′‴		21, 29, 30′, 30″	
23	181.0		3, 5, 24			
24	10.7	1.18 (s)	3, 5			6′, 25
25	14.1	0.75 (s)	1″, 5			1′, 2′‴, 6′, 11′, 24
26	26.8	0.91 (s)	12′/″[b]			11′, 12′
27	15.1	0.86 (d, *J* = 6.8)	14, 15′‴	14	14	12″
28	16.4	1.57 (s)	17, 19′‴			
29	21.4	1.77 (s)	21, 30′‴			21
30	61.5	4.07 (d, *J* = 11.7)/4.17 (d, J = 11.7)	21, 29			

[a] Overlap between C12 and C15

[b] Overlap between C16, C20, and C26

[c] Overlapping multiplets in ^1H

[d] Correlations listed on each receiving carbon row from the denoted proton(s)

Determination of the C14 configuration

Vibrational circular dichroism spectroscopy

In order to relate the measured VCD spectra to the structure, theoretical VCD spectra were simulated computationally. The theoretical modelling focused on the tricyclic system supposedly dominating in VCD spectrum, because a full conformer analysis ($>10^6$ possible conformers) was not possible with available computational means. A reduced ensemble of 27 conformers was generated by 120° rotations around the C13–C14, C4–C23, and C3–O3 bonds only, and relative conformer energies were obtained for both the *R* and *S* C14 isomers. The molecular tail (C14–C30) was kept in the extended conformation and its contribution to VCD was not considered. The equilibrium geometries and spectral properties were calculated using the Gaussian software [24] and the B3LYP/6-311++G**/PCM ($CHCl_3$) level of theory, relative enthalpies were used for property averaging. The simulation reproduced some spectral features observed experimentally (Fig. 4), although the theoretical *R* and *S* VCD sign patterns of **1** are similar. The 1150–1000 cm^{-1} spectral region is however predicted to be significantly

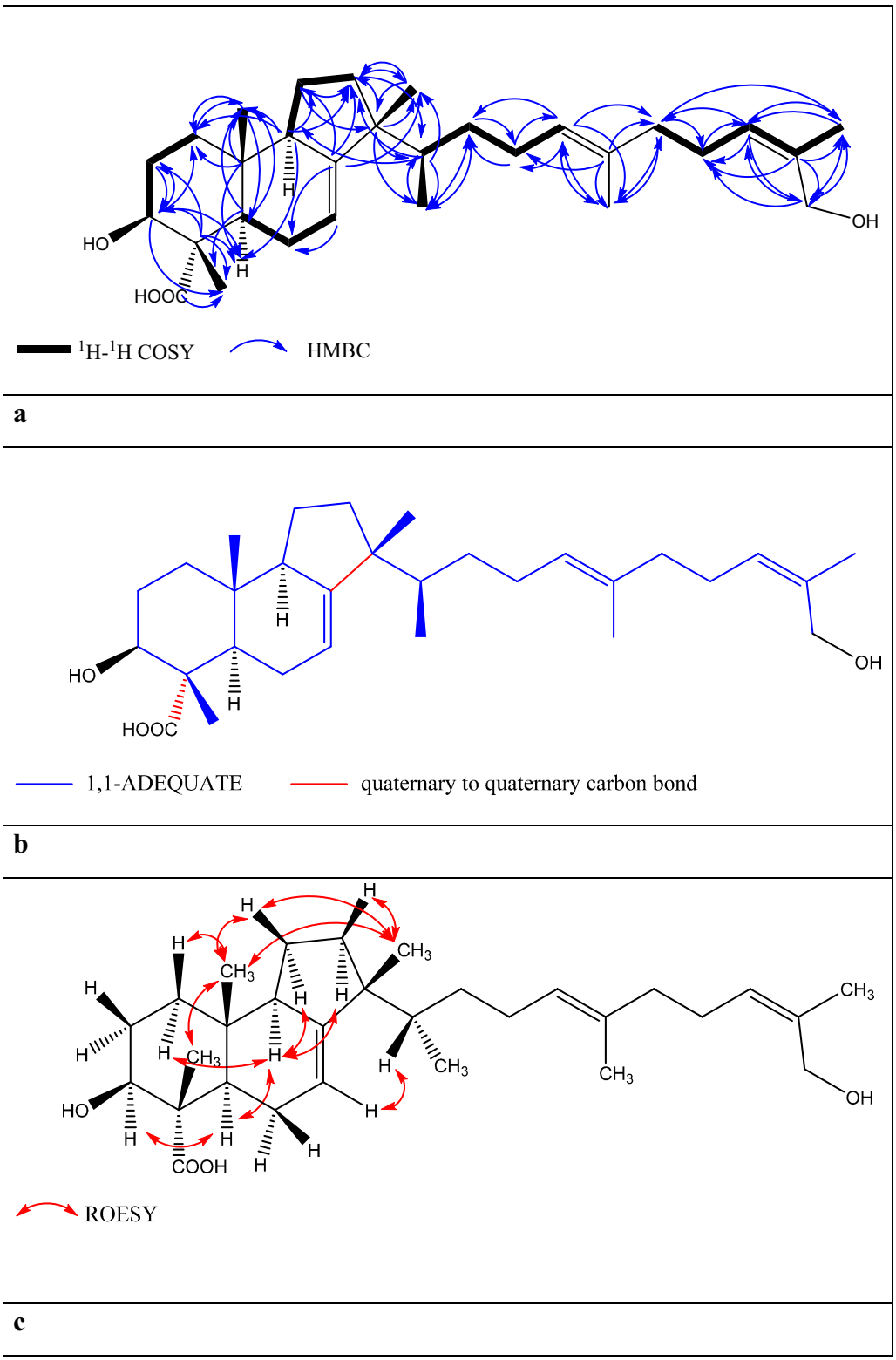

Fig. 3 2D NMR correlations through bonds, **a** COSY, HMBC and, **b** 1,1-ADEQUATE; and through space, **c** NOESY/ROESY of commafric A

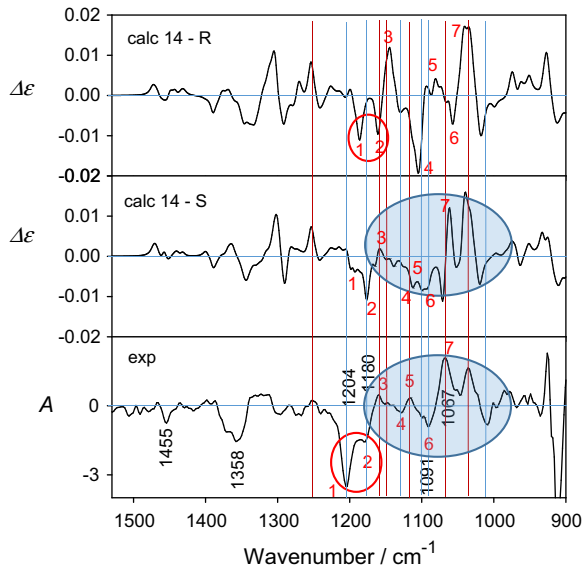

Fig. 4 VCD spectra calculated for the *R* and *S* C14 isomers (upper and middle panels, frequency scaled by 0.967) and the experiment (lower panel). Experimental wavenumbers are denoted in black, and selected bands are assigned identifiers denoted in red. Positive experimental bands are traced with red lines and negative experimental bands are traced with blue lines

Table 2 Calculated C13–C14 angular distribution (*p*, %), for the C14 enantiomers

	R-C14		S-C14	
	p	τ(δεγ)[a]	*p*	τ(δεγ)[a]
Gauche +	12	71.9	11.1	44.9
Gauche −	87.7	− 58.9	11.7	− 64.9
Anti	0.3	− 164.6	77.2	170.6

[a] ∠C26–C13–C14–C27, torsion angle between the two methyl groups as obtained for the optimized DFT geometries

different for the *R*- and *S* configurations, and comparison of the calculated and experimental VCD signs and relative intensities for this region strongly suggests the *S* configuration on C14.

Isotropic NMR parameters

For a more detailed NMR data analysis of distances and coupling constants localized near the C14, only the three Boltzmann averaged rotamers around the C13–C14 bond were used. The H14 proton is preferentially pointing towards the edge of the ring system (and H-7) in both the *R*- and the *S* C14 configurations (Table 2). This was problematic for using the otherwise very informative $^3J_{CH}$ couplings originating from the only proton (H14) directly attached to the rotating C13–C14 bond since

Table 3 Calculated and experimental $^3J_{CH}$ scalar couplings for the C14 enantiomers

	Population	$^3J_{C8H14}$	J_{C12H14}	J_{C26H14}	Configuration
Gauche +	12	0.68	2.12	4.56	R
Gauche −	87.7	0.98	4.6	2.11	
Anti	0.3	4.79	0.82	3.29	
Averaged		0.96	4.38	2.32	
Gauche +	11.1	5.2	3.16	0.87	S
Gauche −	11.7	1.44	1.64	4.41	
Anti	77.2	0.68	4.4	2.55	
Averaged		1.23	3.98	2.57	
Experimental		0.8	5.3	3.7	

[a] ∠C26–C13–C14–C27, torsion angle between the two methyl groups as obtained for the optimized DFT geometries

the dihedral angles formed between the H14–C14 vector and the C13–C8, C12, C26 vectors will be very similar for *R*- and *S*. The predicted differences between the two configurations were smaller than 0.5 Hz. The experimental couplings (Table 3) are in agreement with the calculated rotamer populations of both configurations. These couplings were very challenging to measure accurately experimentally as the signal of H14 overlaps with that of H15s. That made it necessary to use heavily chemical shift filtered selective methods and there is unavoidable phase modulation from J-coupling. Coupling sums were utilized because of significant second order/phase contributions. For all these reasons, the experimental error is estimated to at least 1 Hz.

Furthermore, the possibility to determine the relative configuration from *NOE* buildup rates involving the C27 methyl group were investigated. The C27 methyl group is predicted to be predominantly *anti* to the C26 methyl in the *S*-configuration and *gauche* to the C26 methyl in the *R*-configuration. *NOE* buildups are intrinsically difficult to quantify for flexible molecules due to the fact that they depend on the distance as r^{-6}. A scarcely populated rotamer can contribute significantly to the observed *NOE* if the two protons are positioned very close to each other. The measured *NOE*s around and across the C13–C14 bond (Additional file 1: Fig. S13) are not conclusive alone as both theoretical configurations result in r^2 values in the order of 0.7. However, the most important *NOE* between H26 and H27 that is expected to be the most sensitive to the C14 configuration indicates the *S*-configuration. The weighted experimental *NOE* was determined to $\eta = 0.0054$ (corresponding to $r = 2.9$ Å), *i.e.*, closer to the value predicted for the *S*-model ($\eta = 0.0032$, $r = 3.2$ Å), than that predicted for the *R*-model ($\eta = 0.0144$, $r = 2.5$ Å).

Confirmation of the C14 configuration by anisotropic NMR parameters

Anisotropic NMR parameters have emerged as powerful tools in structural elucidation [35, 36]. Residual dipolar coupling (RDC) depend on the relative orientation of the ^{13}C-^{1}H bond vectors, while residual chemical shift anisotropy (RCSA) depend on the relative orientations of the carbon chemical shielding tensors. When combined, they can provide the configuration of stereogenic centers that are difficult to establish by traditional methods. A method described by Liu et al. [35] utilizing poly(γ-benzyl-L-glutamate) (PBLG) to form a liquid crystal that induces anisotropy in chloroform-d_1 was employed in the present study. ^{13}C residual chemical shifts were referenced to TMS, and combined with RDC data from HSQC-IPAP spectra (Additional file 1: Figs. S14–S16, Tables S1 and S2). In the comparison of the experimental and theoretical anisotropic parameters for the commafric A the *S*-model provided lower quality factors ($Q=0.19$) than the *R*-model ($Q=0.33$, Fig. 5). Based on the anisotropic parameters, together with the VCD and *NOE* data, we conclude that commafric A's stereocenter C14 has the (*S*)-configuration.

Based on the above experimental evidence the structure of the novel compound commafric A was elucidated as (3*S*,4*S*,14*S*,7*E*,17*E*,21*Z*)-3,30-dihydroxypodioda-7,17,21-trien-4-carboxylic acid.

In vitro anti-proliferative effect of the MeOH extract, *n*-hexane fraction, and isolated compounds

The anti-proliferative effects of the crude MeOH extract, *n*-hexane fraction, and isolated compounds commafric A and α-amyrin were tested for four cancer cell lines, A549 (non-small cell lung cancer), A2780 (ovarian cancer), MIA-PaCa-2 (pancreatic cancer), and SNU638 (stomach cancer). The crude methanol extract showed a strong anti-proliferative activity against A549 ($IC_{50}=3.55$ µg/ml) (Table 4, Additional file 1: Fig. S17). The crude extract exhibited weaker activity against A2780, SNU-638, and MIA-Paca-2 compared with A549 cell lines. Among the cell lines tested the methanol crude extract showed strong effect on A549 cell lines (3.55 µg/ml). The *n*-hexane fraction exhibited significant inhibition of cell proliferation on the all four cell lines with dose dependent relationship in vitro. However, it was less sensitive and had a weaker net growth effect on A549 cell lines compared with the crude methanol extract (Table 4, Additional file 1: Fig. S17).

Table 4 IC_{50} values of MeOH extract, *n*-hexane fraction, and isolated compounds of resin of *Commiphora africana* against four cancer cell lines using SRB assay

Sample	Cell lines and IC_{50} (µg/ml)			
	A549	A2780	MIA-PaCa-2	SNU638
MeOH extract	3.55	9.98	19.20	10.09
n-Hexane fraction	9.64	9.62	17.21	10.30
α-Amyrin	9.28	21.96	16.14	28.22
Commafric A	4.52	10.17	10.04	9.73
Etoposide	0.2	0.34	0.42	0.14

IC_{50} (Inhibition of cell growth by 50%), data was generated by experiments performed in triplicates

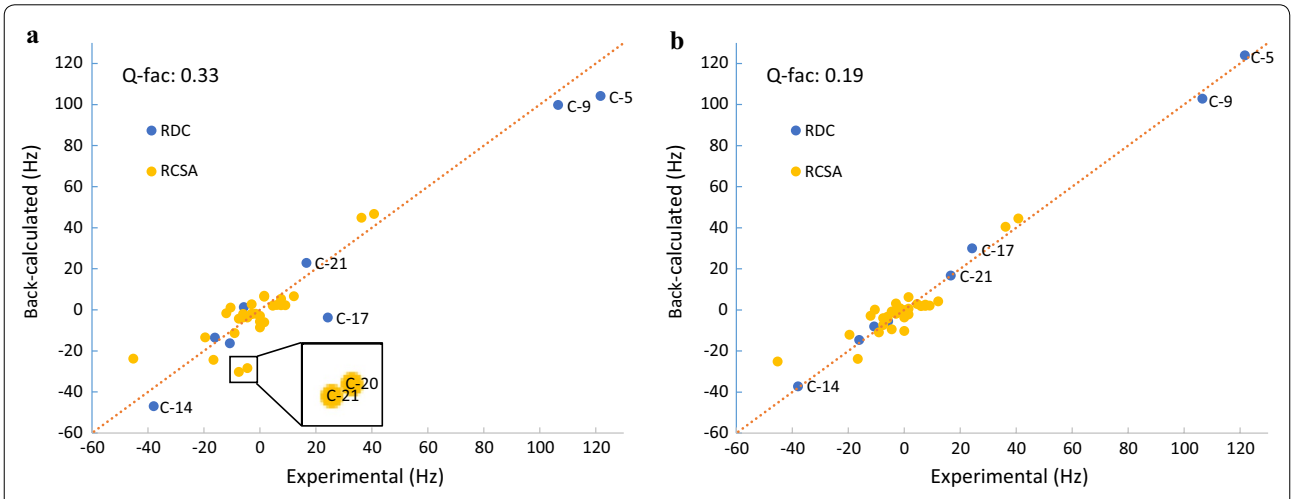

Fig. 5 Stereochemical differentiation between the **a** *R*- and **b** *S* configurations of C14 in commafric A using RDC and RCSA data collected in PBLG, showing the best agreement between experimental and theoretical data for the *S* configuration

Discussion

A number of bioactive compounds were previously reported from different *Commiphora* species. In this study, the *n*-hexane fraction of *C. africana* resin yielded a new compound commafric A. Cancer, cardiovascular diseases, chronic respiratory disorders and diabetes are the primary cause of deaths worldwide. The knowledge of herbal medications and anticancer activity tests assist in the development of important anticancer drugs [37].

In our study for in vitro anti-proliferative activity, we found that the crude extract and related *n*-hexane fraction is lower than 30 µg/ml, which is within the limit of criteria set by the American National Cancer Institute for further purification [38]. For compound **1**, a moderate anti-proliferative activity was observed for the A549 cancer cell lines, with IC_{50} value of 4.52 µg/ml. This is comparable with the activity of the crude extract and more than twice better than for α-amyrin. On the other hand, compound **1** showed weak anti-proliferative effects > 9 µg/ml for the other cell lines. The compound exhibited about twice higher activity on MIA-PaCa-2 compared with the methanol extract. The presence of carboxylic acid or terminal hydroxyl group in the compound might be the reason for its bioactivity. α-Amyrin (**2**) having an ursane skeleton showed weaker activity on A549, A2780, and SNU638 cell lines compared with both compound **1** and the crude methanol extract. Compounds with similar skeleton to α-amyrin such as ursolic acid and its derivatives showed strong anti-proliferative activity against ovarian carcinoma, pancreatic carcinoma, prostate cancer, cervical carcinoma, hepatic cancer, breast cancer, colorectal cancer, leukemia, neuroma, and colon adenocarcinoma [39]. The weak activity of α-amyrin might be due to lack of carboxylic acid group. According to the literature on *α*-amyrin pentacyclic triterpenes stimulate proliferation of human keratinocytes but do not protect them against UVB damage [40–42]. A review on antitumor effect of triterpene acid compounds revealed that triterpene acid type compounds have many effects including anti-inflammatory, regulating blood sugar level, antiviral, and antitumor activity. More important, triterpene acid type compounds have become one of the most popular topics recently because of its selective toxic effects on cancer cells and harmless to normal cells [43].

The tricyclic triterpene acid (3*S*,4*S*,14*S*,7*E*,17*E*,21*Z*)-3,30-dihydroxypodioda-7,17,21-trien-4-carboxylic acid (commafric A) was isolated from the *n*-hexane fraction of the resin of *C. africana* and its structure was determined. It showed the variable IC_{50} values against the four cancer cell lines studied. The anti-proliferative effect against non-small cell lung cancer (A549) cells with IC_{50} values of 4.52 µg/ml was the highest among the cancer cells tested. The anti-proliferative effect suggests that commafric A has a potential in further investigations as a drug against different cancer lines. Further work is required to evaluate the mechanism of action of the commafric A as an antitumor agent against non-small cell lung cancer and evaluate its anti-proliferative on a number of cancer cell lines. Further isolation of compounds from the resin and other parts of this plant will be pursued which might yield some novel bioactive compounds.

Supplementary information

Supplementary information accompanies this paper at https://doi.org/10.1186/s13765-020-00499-w.

Additional file 1. Additional figures and tables.

Abbreviations

HRESIMS: High resolution electrospray ionization mass spectroscopy; SRB: Sulphorhodamine B; VCD: Vibrational Circular Dichroism; RDC: Residual dipolar coupling; RCSA: Residual chemical shift anisotropy; PBLG: Poly(γ-benzyl-L-glutamate).

Acknowledgements

We thank Prof. Ermias Dagne for initiating a research project work on the chemical composition of *Commiphora* resins especially those of Ethiopian origin in his research laboratory and his assistance in this study.

Authors' contributions

WD conducted the experimental studies such as extraction, isolation, characterization of compounds. WD also contributed in drafting the manuscript. PB and EB were involved in VCD analysis. JI and FG performed NMR analysis. JSMS participated in the interpretation of the NMR data and substantially revised the manuscript draft. AJAa supervised the project. SU and SL conducted the bioassay and HRMS analysis. YJ and ZS contributed the crucial help in supervision of the bioassay tests. AD conceptualized, designed and directed the study. All authors read and approved the final manuscript.

Funding

Financial support for this work such as research materials required for extraction, isolation of compounds and cytotoxicity tests was provided by National Research Foundation of Korea (No. 2016K1A3A1A09939937), RDA Troms: TFK2014-207, Norway provided support in materials required for NMR studies. Funding from Digital Life Norway/Research Council of Norway, project ID: 269425, is gratefully acknowledged. Adama Science and Technology University supported for some research materials required for extraction, isolation of compounds and salary of WD and AD. The Czech Grant Agency (18-05770S) provided salary for PB and EB, Ministry of Education (LTC17012 and CZ.02.1.0 1/0.0/0.0/16_019/0000729) provided computational resources. The funders of Grants play no role in the design of the study and collection, analysis, and interpretation of data and in writing the manuscript. All the responsibilities starting from the design of the study up to the write up of the manuscript were undertaken by the authors.

Availability of data and materials

The datasets used and analysed during the current study are available from the corresponding author on reasonable request.

Ethics approval and consent to participate

Not applicable because we did not work with animals or humans.

Consent to publish

Not applicable.

Competing interests

The authors declare that they have no competing interests.

Author details
[1] Department of Applied Chemistry, Adama Science and Technology University, Adama, Ethiopia. [2] Department of Chemistry, UiT the Arctic University of Tromsø, 9037 Tromsø, Norway. [3] Institute of Organic Chemistry and Biochemistry, Academy of Sciences, Flemingovo Náměstí 2, Dejvice, 16610 Prague 6, Czech Republic. [4] Department of Analytical Chemistry, University of Chemistry and Technology, Technická 5, 16628 Prague, Czech Republic. [5] Bio & Drug Discovery Division, Korea Research Institute of Chemical Technology, Daejeon, Republic of Korea. [6] Institute of Pharmaceutical Science, Adama Science and Technology University, Adama, Ethiopia.

Received: 3 January 2020 Accepted: 28 February 2020
Published online: 17 March 2020

References

1. Aziz MM, Raza MA, Saleem H, Wajid M, Bashir K, Ikram M (2014) Medicinal values of herbs and plants, importance of phytochemical evaluation and ethnopharmacological screening: an illustrated review essay. J Pharm Cosmet Sci 2(1):6–10
2. Burkill HM (1994) The useful plants of west tropical Africa. Volume 2: Families EI: Royal Botanic Gardens
3. Adebayo H, Aliyu R, Gatsing D, Garba H (2006) The effects of ethanolic leaf extract of *Commiphora africana* (Burseraceae) on lipid profile in rats. Int J Pharmacol 2(6):618–622
4. Akor J, Anjorin T (2009) Phytochemical and antimicrobial studies of *Commiphora africana* root extracts. Int J Agric Biol 11(6):795–797
5. Abbiw D (1990) Useful plants of Ghana, Intermediate Tech. Publication London, Royal Botanic Gardens, Kew, p 207
6. Worku A, Lemenih M, Fetene M, Teketay D (2011) Socio-economic importance of gum and resin resources in the dry woodlands of Borana, southern Ethiopia. Forests Trees Livelihoods. 20(2–3):137–155
7. Ahmed IM, Gadir SA, Elgilany EE, Abdallah TM (2016) *Commiphora africana* resin phytochemical analysis and some biological aspects. Europ J Med Plant 13(3):1–11
8. Mullauer FB, Kessler JH (2019) Medema JP (2009) Betulin is a potent anti-tumor agent that is enhanced by cholesterol. PLoS ONE 4(4):e1. https://doi.org/10.1371/journal.pone.0005361
9. Aiken C, Chen CH (2005) Betulinic acid derivatives as HIV-1 antivirals. Trends Mol Med 11(1):31–36
10. Brieskorn CH, Noble P (1983) Two furanoeudesmanes from the essential oil of myrrh. Phytochemistry 22(1):187–189
11. Dekebo A, Dagne E, Sterner O (2002) Furanosesquiterpenes from *Commiphora sphaerocarpa* and related adulterants of true myrrh. Fitoterapia 73(1):48–55
12. Dolara P, Luceri C, Ghelardini C, Monserrat C, Aiolli S, Luceri F, Lodovici M, Menichetti S, Romanelli MN (1996) Analgesic effects of myrrh. Nature 379(6560):29
13. Dekebo A, Dagne E, Hansen LK, Gautun OR, Aasen AJ (2000) Crystal structures of two furanosesquiterpenes from *Commiphora sphaerocarpa*. Tetrahedron Lett 41(50):9875–9878
14. Başer K, Demirci B, Dekebo A, Dagne E (2003) Essential oils of some *Boswellia* spp, myrrh and opopanax. Flavour Fragrance J 18(2):153–156
15. Messina F, Gigliarelli G, Palmier A, Marcotullio C (2017) Furanodienone: an emerging bioactive furanosesquiterpenoid. Curr Org Chem 21(4):305–310
16. Nguyen TT, Truong BN, Mai HDT, Litaudon M, Do Thi T, Chau VM, Pham VC (2017) Cytotoxic dammarane-type triterpenoids from the leaves of *Viburnum sambucinum*. Bioorganic Med Chem Lett 27(8):1665–1669
17. Dekebo A, Dagne E, Curry P, Gautun OR, Aasen AJ (2002) Dammarane triterpenes from the resins of *Commiphora confusa*. Bull Chem Soc Ethiopia 16(1):81–86
18. Yan H-J, Wang J-S, Kong L-Y (2014) Cytotoxic dammarane-type triterpenoids from the stem bark of Dysoxylum binecteriferum. J Nat Prod 77(2):234–242
19. Dekebo A, Lang M, Polborn K, Dagne E, Steglich W (2002) Four lignans from *Commiphora erlangeriana*. J Nat Prod 65(9):1252–1257
20. Habtemariam S (2003) Cytotoxic and cytostatic activity of erlangerins from *Commiphora erlangeriana*. Toxicon 41(6):723–727
21. Lodeiro S, Xiong Q, Wilson WK, Kolesnikova MD, Onak CS, Matsuda SP (2007) An oxidosqualene cyclase makes numerous products by diverse mechanisms: a challenge to prevailing concepts of triterpene biosynthesis. J Am Chem Soc 129(36):11213–11222
22. Arai Y, Hirohara M, Ageta H (1989) Fern constituents: three new skeletal triterpenoid hydrocarbons isolated from Polypodiodes niponica. Tetrahedron Lett 30(51):7209–7212
23. Frisch M, Trucks G, Schlegel H, Scuseria G, Robb M, Cheeseman J, Scalmani G, Barone V, Petersson G, Nakatsuji H (2016) Gaussian 16, Revision A. 03, Gaussian, Inc., Wallingford CT
24. Becke AD (1993) Density functional thermochemistry III The role of exact exchange. J Chem Phys 98(7):5648–5652
25. Cossi M, Rega N, Scalmani G, Barone V (2003) Energies, structures, and electronic properties of molecules in solution with the C-PCM solvation model. J Comput Chem 24(6):669–681
26. Stephens P (1987) Gauge dependence of vibrational magnetic dipole transition moments and rotational strengths. J Phys Chem 91(7):1712–1715
27. Stephens P, Ashvar C, Devlin F, Cheesemano J, Frischo M (1996) Ab initio calculation of atomic axial tensors and vibrational rotational strengths using density functional theory. Mol Phys 89(2):579–594
28. Skehan P, Storeng R, Scudiero D, Monks A, McMahon J, Vistica D, Warren JT, Bokesch H, Kenney S, Boyd MR (1990) New colorimetric cytotoxicity assay for anticancer-drug screening. J Nat Cancer Inst 82(13):1107–1112
29. Otuki MF, Ferreira J, Lima FV, Meyre-Silva C, An Malheiros, Muller LA, Cani GS, Santos AR, Yunes RA, Calixto JB (2005) Antinociceptive properties of mixture of α-amyrin and β-amyrin triterpenes: evidence for participation of protein kinase C and protein kinase A pathways. J Pharmacol Exp Ther 313(1):310–318
30. Aragao GF, Carneiro LM, Júnior AP, Bandeira PN, Lemos TL, Viana GS (2007) Antiplatelet activity of α-and β-amyrin, Isomeric mixture from *Protium heptaphyllum*. Pharm Biol 45(5):343–349
31. Vázquez LH, Palazon J, Navarro-Ocaña A (2012) The pentacyclic triterpenes & #x03B1;, β-amyrins: A review of sources and biological activities. In: Vázquez LH (ed) Phytochemicals—A global perspective of their role in nutrition and health. IntechOpen, New York, pp 487–502
32. Saurí J, Parella T, Espinosa JF (2013) CLIP-HSQMBC: easy measurement of small proton–carbon coupling constants in organic molecules. Organic Biomol Chem 11(27):4473–4478
33. Stuppner H, Moller E (1993) Cucurbitacins with unusual side chains from *Picrorhiza kurroa*. Phytochemistry 33(5):1139–1145
34. Tai T, Shingu T, Kikuchi T, Tezuka Y, Akahori A (1995) Triterpenes from the surface layer of *Poria cocos*. Phytochemistry 39(5):1165–1169
35. Liu Y, Cohen RD, Gustafson KR, Martin GE, Williamson RT (2018) Enhanced measurement of residual chemical shift anisotropy for small molecule structure elucidation. Chem Commun 54(34):4254–4257
36. Liu Y, Navarro-Vázquez A, Gil RR, Griesinger C, Martin GE, Williamson RT (2019) Application of anisotropic NMR parameters to the confirmation of molecular structure. Nat Protoc 14(1):217
37. Saleem H, Zengin G, Ahmad I, Lee JTB, Htar TT, Mahomoodally FM, Naidu R, Ahemad N (2019) Multidirectional insights into the biochemical and toxicological properties of *Bougainvillea glabra* (Choisy.) aerial parts: a functional approach for bioactive compounds. J Pharmaceut Biomed 170:132–138
38. Radovanovic A (2015) Evaluation of potential cytotoxic effects of herbal extracts. Serbian J Exp Clin Res 16(4):333–342
39. Chudzik M, Korzonek-Szlacheta I, Król W (2015) Triterpenes as potentially cytotoxic compounds. Molecules 20(1):1610–1625
40. Chaturvedula VP, Schilling JK, Miller JS, Andriantsiferana R, Rasamison VE, Kingston DG (2004) New cytotoxic terpenoids from the wood of vepris p unctata from the Madagascar Rainforest. J Nat prod 67(5):895–898
41. Biskup E, Gołębiowski M, Gniadecki R, Stepnowski P, Łojkowska E (2012) Triterpenoid α-amyrin stimulates proliferation of human keratinocytes but does not protect them against UVB damage. Acta Biochim Pol 59(2):255–260
42. Sun H, Fang W-S, Wang W-Z, Hu C (2006) Structure-activity relationships of oleanane-and ursane-type triterpenoids. Bot Stud 47(4):339–368
43. Zhang W, Men X, Lei P (2014) Review on anti-tumor effect of triterpene acid compounds. J Cancer Res Ther 10(5):14

Publisher's Note